Dynamics of Various Metal-Octaethylporphyrins in Solution Studied by Resonance Raman and Low-Temperature Optical Absorption Spectroscopies. Role of the Central Metal

Antonio Cupane* and Maurizio Leone

Istituto Nazionale di Fisica della Materia (INFM), and Department of Physical and Astronomical Sciences, University of Palermo, Via Archirafi 36, 90123 Palermo, Italy

Esko Unger, Christina Lemke, Michael Beck, Wolfgang Dreybrodt, and Reinhard Schweitzer-Stenner

Institut für Experimentelle Physik, Universität Bremen, 28359 Bremen, Germany

Received: December 1, 1997; In Final Form: April 8, 1998

The temperature dependence of the Soret band of various metal-octaethylporphyrins [i.e., Ni(II), Cu(II), and Pd(II)] dissolved in the glass-forming mixture 50% (v/v) isopentane/ethyl ether in the temperature range 300−40 K was studied. Co(II)-octaethylporphyrin dissolved in dichloromethane was also investigated in the temperature range 300−180 K. The aim of the work was to investigate the role of the central metal in the conformational flexibility of porphyrins and in communicating solvent motions to their macrocycle. We used resonance Raman spectroscopy to determine the vibronic coupling of high-frequency modes to the electronic transition into the porphyrin B state. The corresponding coupling of a "bath" of low-frequency porphyrin/solvent motions was taken into account by a temperature-dependent Gaussian width (σ) of the Soret band. Following the approach of Melchers et al. (*Biophys. J.* **1996**, *70*, 2092−2099), the mean square fluctuations (MSF) of the central metal atom with respect to the porphyrin plane were determined from the σ temperature dependence. MSF values exhibited a harmonic behavior only at low temperatures, whereas an increase of the MSF well above the predictions of the harmonic model was observed above the glass transition temperature of the solvent mixture. This result was rationalized by invoking coupling of solvent motions to the vibrations of the central metal atom. The magnitude of this coupling is strongly metal dependent in that it is large for Ni(II) and Pd(II), weak for Co(II), and almost negligible for Cu(II). This dependence is discussed in terms of the ionic radii and electronic structure of the various metals. Moreover, for Ni(II), we found the MSF to have an amplitude comparable with what has earlier been obtained for iron-heme complexes in proteins and in solution.

Introduction

Metalloporphyrins serve as reactive sites in various biological systems in that they bind axial ligands in transport proteins, support light harvesting, accept and donate electrons and catalyze biochemical reactions.[1] Additionally, porphyrins become increasingly relevant in applied chemistry where they have been chemically cross-linked to yield highly efficient electron-transfer systems.[2] Therefore, a detailed understanding of their structural and dynamic properties as well as their physical and chemical basis is highly warranted.

Recent spectroscopic studies have revealed that the porphyrins are very flexible, so they can adjust their structure to external forces.[3] This capability makes porphyrins ideal for serving as active sites in proteins, where they accommodate multiple noncovalent interactions imposed by the amino acid side chains constituting their mostly hydrophobic environment. As a consequence, many porphyrin macrocycles in proteins, such as cytochrome c, hemoglobin, and myoglobin exhibit nonplanar structures that are suspected to affect the efficiency and rates of their biological function.[4] The latter, however, mainly depends on the electronic structure and dynamics of the central metal atom (Fe or Cu ions). Thus, the porphyrins functional properties are to a major extent determined by interactions between macrocycle and metal, in that structural changes of the former alter the ligand crystal field of the latter. On the other hand, the structure of the macrocycle may depend on the metal size and electronic properties. Ni(II)-porphyrins with peripheral substituents, for instance, prefer a nonplanar conformation due to the small ionic radius of the metal that forces the pyrroles into closer proximity to optimize the N−Ni(II) bond distance. This motion encounters some strain due to nonbonded interactions between the pyrroles, which is minimized by tilting and twisting with respect to the macrocycle mean plane to allow N−Ni(II) bond lengths close to the "optimal" value.[3]

An understanding of the relationship between porphyrin structure and function requires studying metal−porphyrin as well as porphyrin−environment interactions. In proteins, the latter is provided by amino acid residues in more or less well-defined secondary structure; in organic solvents, environmental molecules are smaller and less restricted in their translational and rotational motions. For both systems, it is not sufficient to explore the static forces involved; additionally, one has to elucidate all aspects of intra- and intermolecular dynamics. For

* Corresponding author. Phone: +39-91-6234220. Fax: +39-91-6162461. E-mail: cupane@fisica.unipa.it.

S1089-5647(98)00362-9 CCC: $15.00
Published on Web 07/15/1998

porphyrins, these aspects include the influence of phonon-like solvent motions on optical and vibrational properties of the macrocycle. The former yields a temperature-dependent broadening of the optical absorption bands,[5] whereas the latter gives rise to dephasing of vibrational excited states monitored by resonance Raman scattering.[6]

In a series of papers from one of our laboratories,[5] a model was developed to quantitatively analyze optical bands of chromophores in solvents and protein environments, which are exclusively determined by Franck−Condon type transitions into the vibronic manifold of the respective excited state. In this approach, each vibronic transition is described by a Voigtian profile arising from convoluting a temperature-independent Lorentzian with a temperature-dependent Gaussian part. The latter is thought to arise from a bath of low-frequency modes vibronically coupled to the electronic transition under consideration. Several studies on metalloporphyrins in heme proteins[5] as well as in solvents[7] have provided evidence that these low-frequency motions become anharmonic at temperatures above the glass transition of the porphyrin environment. This anharmonicity yields a much stronger increase of the Gaussian half-width with rising temperature than theoretically predicted for the harmonic case. As shown by Leone et al. in 1994,[7b] this thermal broadening effect is absent in metal-free porphyrins, thus indicating a central role of the metal for the coupling of phonon-like matrix motions to porphyrin electronic transitions.

This possible central role of metals motivated us to study and compare the optical properties of octaethylporphyrins (OEPs) with metal atoms differing both in size and electronic properties. To this end we measured the Soret band of Cu(II)-OEP and Pd(II)OEP dissolved in the glass-forming mixture 50% (v/v) isopentane/ethyl ether (IPEE) and of Co(II)OEP dissolved in dichloromethane (DCM), as a function of temperature between 40 and 300 K and between 180 and 300 K, respectively. To simplify the analysis of the vibronic sidebands we also recorded Raman spectra with Soret excitation, from which a set of relative coupling parameters was derived for Franck−Condon active A_{1g} modes. Finally, the temperature dependence of the band parameters of the aforementioned OEPs were compared with those earlier obtained for Ni(II)OEP dissolved in IPEE.[7a] Our results underscore the pivotal role of the motions involving the metal atom in transducing anharmonic motions of the environment to the chromophore.

Materials and Methods

Materials. NiOEP, CuOEP, CoOEP, and PdOEP were purchased from Sigma Chemie. Purification and sample homogeneity controls were performed as described earlier.[8] Carbon disulfide, isopentane, ethyl ether, and dichloromethane were purchased from Fluka and were of UV spectroscopy grade. CS_2 was used as solvent for all Raman experiments.

Resonance Raman Spectroscopy. The Raman instrumentation is described in detail elsewhere.[8] Briefly, the polarized Raman spectra of Cu(II)OEP were recorded with the CW excitation (406.7 nm) provided by a Krypton ion laser (Coherent, Innova 90 K). The measurements were performed with backscattering geometry. By using a cylindrical lens of 10-cm focal length, the linear polarized beam was focused onto the sample. The scattered light was collected and imaged on the entrance slit of the spectrometer (i.e., a Spex 1401 double monochromator equipped with 1200 grooves/mm gratings), and detected by a CCD camera. Polarized Raman spectra were observed with a polarization filter as analyzer placed in front of the entrance slit of the spectrometer followed by a scrambler. The entrance slit was adjusted to 100 μm; the corresponding slit width at the wavelength employed was 2.5 cm^{-1}. Measurements were carried out both at 290 and 220 K.

The polarized Raman spectra of Pd(II)OEP and of Co(II)-OEP were recorded with an excimer pumped dye laser with 425 nm excitation. The pulse energy was 1 mJ at a 200 Hz repetition rate and a pulse length of ≈10 ns. The average laser power at the sample was between 30 and 100 mW. The incident beam was polarized parallel to the spectrometer entrance slit, filtered by two pinholes, and focused by a cylindrical lens of 40-cm focal length onto a spinning quartz cell. The measurements were carried out at room temperature (290 K). A polarization filter and a scrambler were again used to observe polarized spectra. The scattered light was dispersed by a 500-nm blazed SPEX triple monochromator 1402 equipped with a 1200 groove/mm grating and detected by a CCD camera. This system provides 512 channels for data acquisition, thus covering a spectral range of 14.2 nm. All data acquired by the set ups just described were stored in an IBM-AT computer for further analysis. The polarized Raman spectra of Ni(II)OEP were measured at 290 K as described by Jentzen et al.,[8] and they are the same as those previously reported.[7a]

Analysis of Raman Spectra. All spectra were transferred to a personal computer and subjected to a line shape analysis by the recently developed program MULTIFIT.[9] This program allows appropriate baseline corrections, decomposition of highly overlapping bands, deconvolution of the spectrometer function, and discrimination between Lorentzian, Gaussian, and Voigtian band profiles.[8,9] All spectra shown in this paper are normalized on the internal standard (i.e., the ν_1 band of CS_2 at 656 cm^{-1}). The spectra were corrected for sample reabsorption and also for the factor $\nu_{EXC}(\nu_{EXC} - \nu_j)^3$, where ν_{EXC} is the excitation frequency and ν_j denotes the Raman shift. The intensities of the normalized polarized Raman bands were derived from their band areas.

Optical Absorption Spectroscopy. Spectra in the range between 500 and 300 nm were recorded in digitized form at 0.5-nm intervals with a PC−IBM-controlled Cary Varian 2300 spectrophotometer. The scan speed was 0.5 nm/s, the integration time was 0.5 s, and the slit width was <0.2 nm in the whole wavelength range, corresponding to a spectral resolution of ≈15 cm^{-1} at 400 nm.

The experiments were performed with CuOEP and PdOEP dissolved in a 50% (v/v) mixture of isopentane and ethyl ether (IPEE) at various temperatures between 300 and 40 K. For CoOEP, dichloromethane (DCM) was used as a solvent because spectroscopically inhomogeneous samples were obtained with other solvents; in this case, the temperature range was limited to 300−180 K because of solvent crystallization. The spectra of NiOEP dissolved in IPEE were taken from a previous publication.[7a] Samples were cooled at a rate of 1.5 K/min and were kept at each temperature for equilibration; thermal cycling yielded fully reproducible results. Baselines (cuvette + solvent) were measured as a function of temperature in separate experiments and subtracted from the spectra. The reader may refer to a previous publication[11] for details on the experimental setup. For the sake of comparison with resonance Raman results, optical absorption spectra were also measured for the aforementioned metal-OEPs in CS_2. In this case, the wavelength region was limited to 500−375 nm, because of the high solvent absorption at lower wavelengths. Moreover, the temperature could not be lowered below 170 K, again because of solvent crystallization. In particular, the spectra of the various metal OEPs dissolved in CS_2 measured at 290 K were used, together

with resonance Raman data, to obtain the relative values of the linear coupling constants of the various A_{1g} modes (vide infra).

Optical Absorption Analysis. The resonance Raman spectra of CuOEP, CoOEP, and PdOEP do not indicate the existence of multiple conformers. We therefore assumed that their Soret bands can appropriately be described by a series of vibronic sidebands due to the Franck−Condon type transitions into the two lowest vibronic B-states. Thereby we considered several "high-frequency" A_{1g} type modes of the porphyrin macrocycle, as well as a bath of low-frequency modes that, as we will argue later, can be related to the phonon spectrum of the solvation shell. As a consequence, the apparent band profile is Voigtian and reads as

$$A(\nu) = M_{gB}{}^2 \nu [L(\nu) \otimes G(\nu)] \tag{1}$$

where M_{gB} is a constant proportional to the electronic dipole matrix element, ν denotes the frequency, and $L(\nu)$ is the Lorentzian part of the band shape. The Lorentzian part can be written as

$$L(\nu) = \sum_{\{m_j\}} \left\{ \left[\prod_{j=1}^{N_b} \frac{S_j^{m_j} e^{-S_j}}{m_j!} \right] \frac{\Gamma}{[\nu - \nu_0(T) - \sum_{j=1}^{N_h} m_j \nu_j]^2 + \Gamma^2} \right\} \tag{2}$$

where Γ is a damping factor, which depends on the finite lifetime and the dephasing of the excited state, and N_h denotes the number of high-frequency modes vibronically coupled to the electronic transition. The product extends to all high-frequency porphyrin vibrations ($h\nu_j > k_B T$, where k_B denotes the Boltzmann constant) that are Franck−Condon active in the B state. The sum runs over their occupation numbers m_j. Vibronic coupling of the "high-frequency" porphyrin modes to the electronic transition is described by the linear coupling constants S_j . The term $\nu_0(T)$ is the pure electronic energy difference between the ground state and the excited B state.

As we have shown in previous papers,[5] the electronic transition just mentioned is also vibronically coupled to a "bath of low frequency modes" ($h\nu_j \leq k_B T$). This coupling is accounted for by an Einstein oscillator model that, in the short time limit, yields a Gaussian broadening of the Soret band and is described by the second term, $G(\nu)$, in eq 1:

$$G(\nu) = \frac{1}{\sigma(T)} \exp\left[-\frac{\nu^2}{2\,\sigma^2(T)} \right] \tag{3}$$

where $\sigma(T)$ is the temperature-dependent half-width. "Low-frequency modes" are those whose vibrational frequency is of the same order of, or smaller than, $k_B T$. Consequently, transitions from excited vibrational states are no longer negligible. As we will argue in the *Discussion*, these modes can be assigned mainly to the phonon spectrum of the porphyrin solvation shell.

The procedure adopted to analyze the Soret band profile of NiOEP has been reported previously.[7a] Resonance Raman data[8] led us to assume that the optical band is composed of two subbands, Sb_1 and Sb_2, due to the existence of porphyrin conformers with planar and nonplanar (ruffled) macrocycles, respectively. For each individual subband, the band profile is again described as the convolution of two profiles $L_i(\nu)$ and $G_i(\nu)$, where ($i = 1, 2$).

If one considers the low-frequency bath just mentioned as a set of N degenerate harmonic oscillators with an average coupling constant S and an average frequency $\langle\nu\rangle$ (harmonic Einstein approximation), the temperature dependence of the Gaussian width [parameter $\sigma(T)$ in eq 3] is given by

$$\sigma^2_{harm}(T) = NS\langle\nu\rangle^2 \coth\left[\frac{h\langle\nu\rangle}{2k_B T}\right] + \sigma_{in}{}^2 \tag{4}$$

The subscript "harm" indicates that eq 4 is only valid in the harmonic regime. The term σ_{in} reflects an eventual temperature-independent inhomogeneous broadening, modeled as a Gaussian distribution of 0−0 transition frequencies.

In the presence of quadratic coupling, parameter ν_0 becomes temperature dependent also. Within the harmonic approximation, its thermal behavior can be expressed as

$$\nu_0(T) = \nu_{00} - \frac{1}{4} N\langle\nu\rangle(1 - R) \coth\left[\frac{h\langle\nu\rangle}{2k_B T}\right] + C \tag{5}$$

where R is an effective quadratic coupling constant, ν_{00} is the frequency of the purely electronic (0−0) transition, and C accounts for other temperature-independent contributions to the peak position of the band.

Results and Discussion

Resonance Raman Spectroscopy. Figure 1 shows the polarized resonance Raman spectra of the various metal-OEP derivatives investigated. All spectra were taken in CS_2 at 290 K. All excitation wavelengths indicated in the figure legend are very close to the respective Soret band maxima. For CuOEP, analogous spectra have also been measured at 220 K. A detailed spectral analysis revealed the following information:

(1) As reported previously,[8] the prominent core size marker bands ν_{10}, ν_{19}, and ν_2 in the Raman spectra of NiOEP comprise two subbands due to the coexistence of discrete conformers with planar and nonplanar macrocycle structures. This inhomogeneity becomes evident by the considerably large apparent bandwidth (e.g., 20 cm^{-1} for ν_{10}). In contrast, this Raman band appears with a much narrower half-width of 10 cm^{-1} in the spectra of CuOEP, CoOEP, and PdOEP. The spectral analysis revealed that all these bands can be fitted with a single Lorentzian band, which indicates that these samples are homogeneous with respect to the porphyrin structure. The ν_8 doublet in the spectra of CuOEP reflects conformers with different ethyl orientations that do not exhibit different degrees of nonplanarity. This assessment emerges from the observation that the corresponding resonance excitation profiles do not show any shift of the resonance positions, as it is obtained for the sub-lines of the core size marker bands of NiOEP[8] and NiTPP (Ni(II)tetraphenylporphyrin).[9]

(2) The Raman spectra in Figure 1 are dominated by polarized bands resulting from A_{1g} modes of the porphyrin macrocycle. Because the excitation wavelength is close to the resonance position of the *B* transition, the Raman cross section is governed by intrastate Franck−Condon-type coupling.[10,12] In this case, the relative values of the coupling constants S_j can be obtained with a simplified version[13] of the "transform theory",[14,15] which predicts the following relationship between Raman and absorption cross section:

$$I_j(\nu_{EXC}) = \text{const}(\nu_{EXC} - \nu_j)^3 \nu_{EXC}(n_j + 1) S_j |\alpha_j(\nu_{EXC})|^2 \tag{6}$$

where I_j (ν_{EXC}) is the intensity of Raman scattering for the j-th vibrational mode at frequency ν_j polarized parallel to the incident polarization; ν_{EXC} is the excitation frequency, S_j is the linear

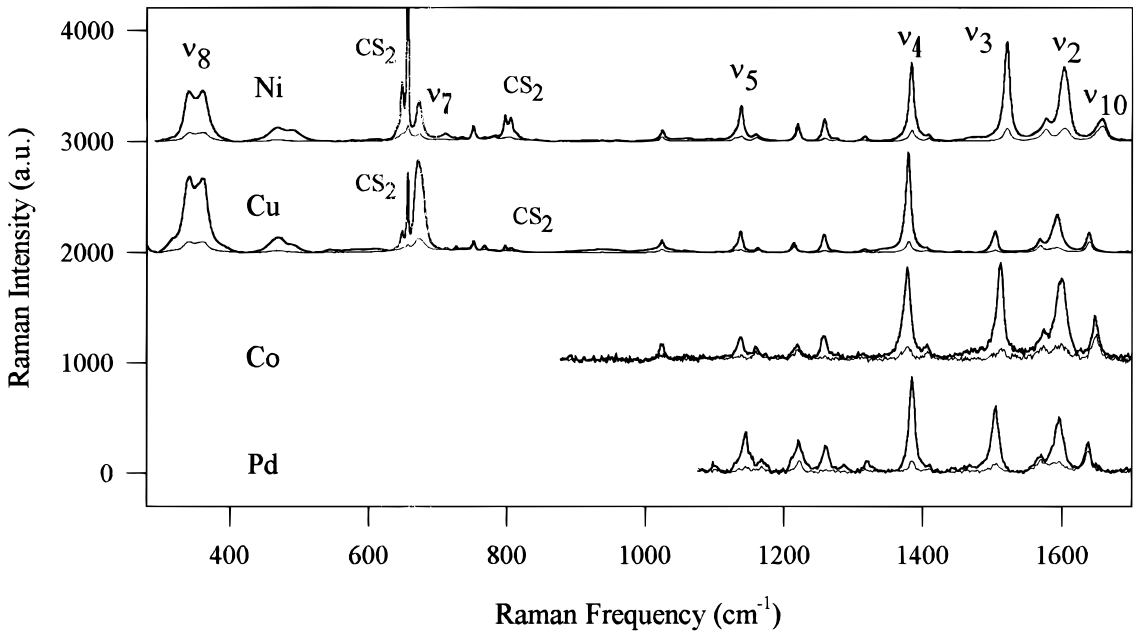

Figure 1. Resonance Raman spectra of metal-OEPs in CS_2 at 290 K. Excitation wavelengths are 406.7 nm for CuOEP and NiOEP, and 425 nm for PdOEP and CoOEP. Soret absorption maxima in CS_2 at 290 K are observed at 404 nm for Ni- and CoOEP, at 407 nm for PdOEP, and at 411 nm for CuOEP.

Franck−Condon coupling constant, and n_j is the occupation number of the vibrational oscillator in the electronic ground state. The quantity $\alpha_j(\nu_{EXC})$ is defined as:

$$\alpha_j(\nu_{EXC}) = \Phi(\nu_{EXC}) - \Phi(\nu_{EXC} - \nu_j) \tag{7}$$

with

$$\Phi(\nu_{EXC}) = \pi^{-1} P \int \frac{\epsilon(x)}{[x(x - \nu_{EXC})]}\, dx + i\frac{\epsilon(\nu_{EXC})}{\nu_{EXC}} \tag{8}$$

where $\epsilon(x)$ is the absorbance at frequency x, and the symbol P indicates that the principal value of the integral has to be calculated. The depolarization ratio does not significantly deviate from its D_{4h} value of 0.125;[16] hence, $I_{j||}(\nu_{EXC}) = 0.83\, I_j(\nu_{EXC})$ for all A_{1g} type modes, where $I_{j||}$ is the area of the j-th Raman line measured parallel polarized to the incident polarization. Therefore, from eqs 6−8 and by measuring the resonance Raman and the optical absorption spectrum at the same temperature and in the same solvent, the relative values of the linear coupling constants can be obtained. Indeed, from eqs 6−8 it follows that

$$\frac{S_j}{S_k} = \frac{A_{j||}}{A_{k||}} \frac{(n_k + 1)}{(n_j + 1)} \frac{|\alpha_k(\nu_{EXC})|^2}{|\alpha_j(\nu_{EXC})|^2} \tag{9}$$

where A_j and A_k are the absorption-corrected Raman band areas. In eq 9 the terms $(\nu_{EXC} - \nu_j)^3$ and $(\nu_{EXC} - \nu_k)^3$ were dropped because, as already mentioned, the Raman bands in Figure 1 were normalized on the internal standard. As a reference, we utilized the well-known Raman band at ≈1379 cm^{-1} (ν_4); the corresponding values of $S^*_j = S_j/S_{1379}$ are reported in Table 1.

Optical Absorption Spectroscopy. Figure 2 shows the spectra of CuOEP, PdOEP, and NiOEP in IPEE and of CoOEP in DCM measured at the indicated temperatures. For all porphyrins investigated, marked changes of the band shape occur as the temperature is lowered from 300 K; that is, the maximum absorbance increases, the bands shift to the red, and vibronic structures emerge at the high energy side. The appearance of a vibronic structure is particularly evident for CuOEP because of the narrow width of the Lorentzian part of its band shape.

TABLE 1: Relative Coupling Constants of A_{1g} Modes for Soret Excitation Obtained from the Resonance Raman Spectra Shown in Figure 1 by the Transform Theory[a]

derivative	S_{1379}	S^*_{1594}	S^*_{1504}	S^*_{1138}	S^*_{674}	S^*_{471}	S^*_{350}	S^*_{269}
CuOEP; $T = 290$ K		0.7	0.25	0.34	1.5	0.35	5.7	1.8
CuOEP; $T = 220$ K		0.65	0.25	0.38	1.7	0.37		
NiOEP; $T = 290$ K		1.3	1.3	0.5	0.8	0.39	3.5	
CoOEP; $T = 290$ K		0.9	0.8	0.2				
PdOEP; $T = 290$ K		0.8	0.6	0.4				

[a] See text for details; S_j^* is defined as $S_j^* = S_j/S_{1379}$.

In agreement with results from resonance Raman spectroscopy, the Soret band of NiOEP has been analyzed in terms of two different subbands arising from a planar and a ruffled conformer, respectively (cf. refs 7a and 8 for more detail). In contrast, the resonance Raman data show only one conformer for CuOEP, CoOEP, and PdOEP, in that their core size markers appear as single bands with a narrow Lorentzian band shape. Therefore, we analyzed the Soret bands of these molecules in terms of a single band with eqs 1−3. The fits to the Soret bands of CuOEP measured at 43 K and of CoOEP measured at 180 K are shown in Figures 3a and b, respectively. The fits are satisfactory, as judged from the residuals depicted in the upper panels. Fits to all the other spectra measured in this study are of comparable or better quality.

From the analysis just presented, essentially two types of information are obtained:

1. Vibrational Coupling and Lifetime of the Excited B State. The corresponding parameters, namely, the relative linear Franck−Condon coupling constants (S_j *) of the high-frequency modes and the homogeneous width (Γ), are listed in Table 2. The validity of our analysis is underscored by the fact that for all porphyrins both S_{1379} and the relative coupling constants S_j*

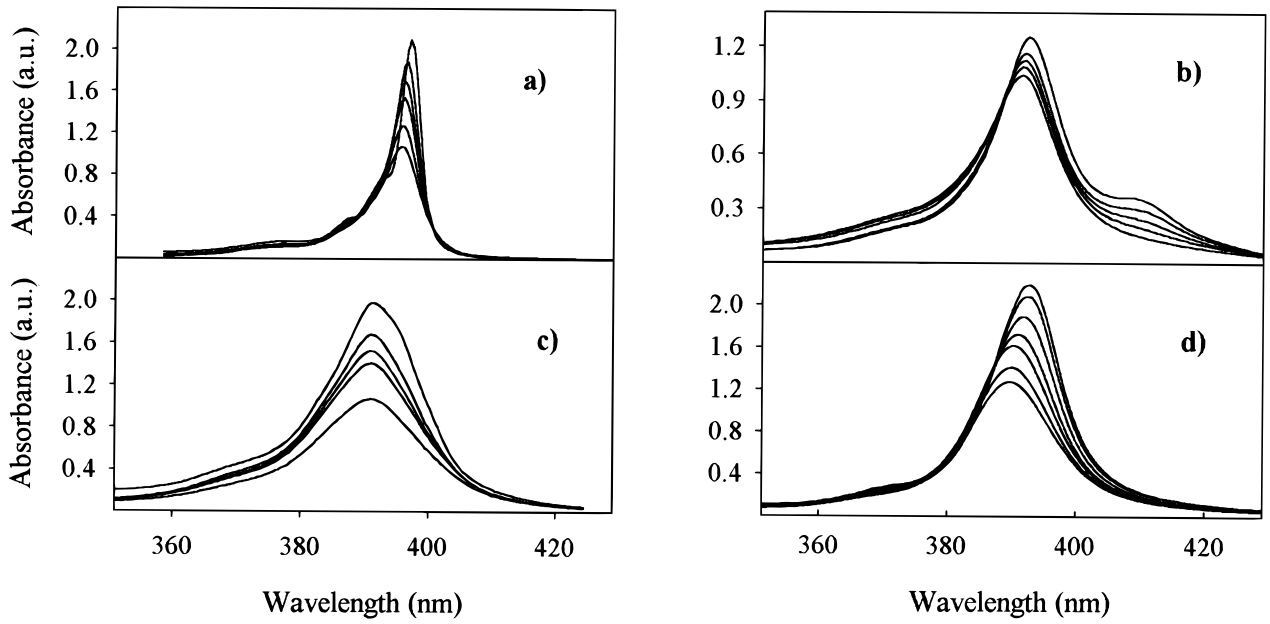

Figure 2. Soret bands of metal-OEPs at various temperatures. (a) CuOEP; from top to bottom, $T = 70$, 170, 200, 230, 270, and 298 K. (b) CoOEP; from top to bottom, $T = 180$, 220, 240, 280, and 300 K. The band in the low-frequency side of the Soret absorption is likely due to some impurity in our sample; it has therefore been subtracted prior to spectral analysis. (c) PdOEP; from top to bottom, $T = 80$, 170, 200, 240, and 300 K. (d) NiOEP; from top to bottom, $T = 40$, 100, 170, 200, 260, and 300 K (data taken from ref 7a). The solvent is IPEE for Cu-, Pd-, and NiOEP, and DCM for CoOEP.

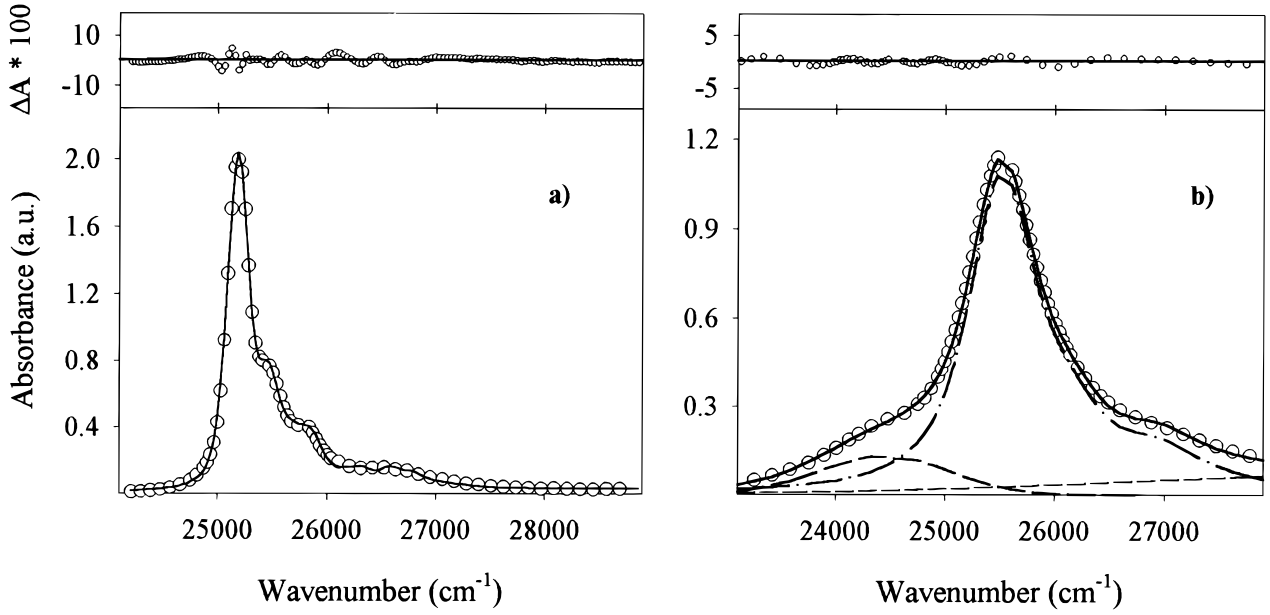

Figure 3. (a) Fitting of the Soret band of CuOEP in IPEE at 40 K. Circles are the experimental points. Not all the experimental points have been reported for the sake of figure readability. The continuous line is the band profile calculated according to eqs 1−3. The residuals are also shown in the upper panel, on an expanded scale. (b) Fitting of the Soret band of CoOEP in DCM at 180 K. Symbols as in panel a. Dashed lines are Gaussian bands that take into account the high-frequency N band and a low-frequency band attributed to some impurity in the sample (see the legend of Figure 2). The dashed−dotted line is the band profile calculated according to eqs 1−3. The solid line represents the overall spectral profile.

of the remaining high-frequency modes emerge as temperature independent from the fitting procedure (see the S_{1379} and S_j* values of CuOEP listed in Table 2), in accordance with physical expectation and with previous observations on hemeproteins.[18] This result in particular demonstrates that even the spectra measured at high temperatures, where the vibronic structure is smeared out by thermal broadening, are fitted in a physically meaningful way.

Some further conclusions can be drawn from the parameters in Table 2. Although relatively large homogeneous width Γ values of ≈300 cm^{-1} are obtained for Co-, Ni- and PdOEP, a much smaller value of ≈70 cm^{-1} emerges from the analysis of CuOEP absorption. Generally, the *B* state is thought to decay rapidly via the pathway $^1B \rightarrow {}^3B \rightarrow {}^3(d_{z^2}, d_{x^2-y^2})$.[17] This observation therefore suggests that intersystem crossing is more efficient for NiOEP than for CuOEP, which indicates a more stabilized triplet state for the latter.

The Franck−Condon coupling constants in Table 2 suggest that due to the narrow Lorentzian width, the vibronic structure of CuOEP is much better resolved (see Figures 2 and 3). This allows an unambiguous estimation of almost all the linear Franck−Condon coupling constants and therefore a direct

TABLE 2: Spectral Parameters Obtained from Fits of the Soret Band of the Various Metal-OEPs[a]

derivative	S_{1379}	S^*_{1594}	S^*_{1504}	S^*_{1138}	S^*_{674}	S^*_{471}	S^*_{300}[b]	Γ (cm^{-1})
CuOEP $T = 290$K	0.03 ± 0.01	0.62[c]	0.22[c]	0.7 ± 0.3	2.2 ± 0.5	2.3 ± 0.6	7 ± 1	110 ± 10
CuOEP $T = 220$K	0.03 ± 0.01	0.62	0.22	0.8 ± 0.3	2.2 ± 0.5	2.2 ± 0.6	7 ± 1	90 ± 10
CuOEP $T = 50$K	0.03 ± 0.01	0.62	0.22	0.8 ± 0.3	2.9 ± 0.5	2.6 ± 0.6	8 ± 1	60 ± 10
NiOEP $T = 40$K	0.05 ± 0.01[d]				>0.1[e]		3.5 ± 0.5	335 ± 20
CoOEP $T = 200$K	0.08 ± 0.01[d]				1.6 ± 0.5		1.3 ± 0.2	300 ± 20
PdOEP $T = 40$K	0.09 ± 0.01[d]				2.0 ± 0.5			245 ± 20

[a] For the modes at 1594, 1504, 1138, 674, 471, and 300 cm^{-1}, relative linear coupling constants (S_j*) are reported, to allow direct comparison with data from resonance Raman spectroscopy (see Table 1); solvent is DCM for CoOEP and IPEE for all the other porphyrins. [b] The average "mode" at 300 cm^{-1} takes into account the coupling with both ν_8 (at $\approx$350 cm^{-1}) and ν_9 (at $\approx$270 cm^{-1}); for NiOEP and CoOEP, an average "mode" at 350 cm^{-1} was used. [c] To reduce the number of adjustable parameters, values of S^*_{1594} and of S^*_{1504} were not optimized during the fits. [d] In view of the rather large Γ values, an average "mode" at $\approx$1520 cm^{-1} was used for these derivatives (see text). [e] For NiOEP, coupling with the mode at 674 cm^{-1} (ν_7) was undetectable with optical absorption spectroscopy.

comparison with resonance Raman results. We find a value of $S_{1379} = 0.03$, in good agreement with previously reported data on the coupling strength of ν_4 to the Soret absorption in hemeproteins.[18] Moreover, all relative S_j* values are in good agreement with the analogous data from resonance Raman spectroscopy reported in Table 1. One exception is the band observed at 471 cm^{-1}, which is attributed to vibrations of the peripheral ethyl groups. Its relative coupling value as obtained from Soret absorption (2.2) is a factor of 5 larger than that obtained from resonance Raman (0.4). This discrepancy may arise from different interactions between the ethyl substituents and the respective solvent (IPEE for optical spectroscopy; CS_2 for resonance Raman spectroscopy). A representative vibration with a frequency of 300 cm^{-1} was assumed to account for the modes at 269 cm^{-1} (ν_9) and 350 cm^{-1} (ν_8) whose frequency difference is smaller than Γ. The relative value of the coupling strength of this effective mode agrees fairly well with the sum of the relative coupling strengths of ν_8 and ν_9 reported in Table 1.

Finally, with regard to vibronic sidebands, the rather large Γ values for Ni, Co, and PdOEPs, make it impossible to separately resolve the vibronic structure arising from modes with frequencies close to each other. We therefore used effective modes to account for the coupling with the various frequency regions. Despite this limitation, there is general agreement between the optical absorption and resonance Raman data, even in fine details. In fact, the higher coupling obtained for the effective mode at 1520 cm^{-1} of Ni-, Co-, and PdOEP compared with the corresponding value for CuOEP reflects well the higher intensity of the Raman spectra in this frequency region, which exhibits the relatively intense Raman bands ν_2 and ν_3. For NiOEP, the analysis of optical absorption does not reveal any significant coupling for ν_7 at $\approx$674 cm^{-1}, which is in agreement with the low intensity of this band in the Raman spectrum. Finally, both Raman and optical absorption data consistently indicate that the coupling strength of an effective mode at 350 cm^{-1} is larger by a factor of 2 for CuOEP compared with NiOEP.

2. Dynamic Properties. Figures 4 and 5 show the temperature dependence exhibited by the Gaussian half-widths and peak frequencies of the Soret bands (parameters σ^2 and ν_0) of the metal-OEPs investigated. The solid lines in Figures 4 and 5 result from a fit of eqs 4 and 5 to the low-temperature data points. Values of the relevant parameters, which characterize the coupling of the electronic Soret transition to the "bath" of low-frequency modes, are listed in Table 3. Significant deviations from the predictions of the harmonic Einstein approximation become evident at high temperatures. These deviations are visualized in Figure 6, which displays $\Delta\sigma^2(T) = \sigma^2(T) - \sigma^2_{harm}(T)$; that is, the differences between the experimentally obtained σ^2 values and the solid lines representing the fit of the harmonic model to the low-temperature data (see Figure 4). For NiOEP, the appearance of deviations from the harmonic behavior at temperatures >120 K has already been reported[7a] and has been attributed to the onset of anharmonic

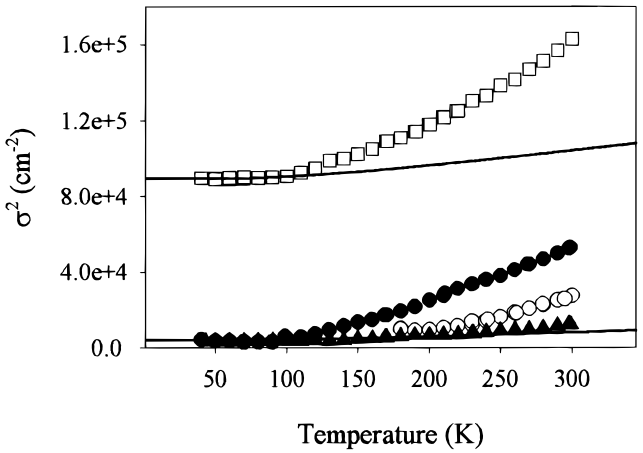

Figure 4. Values of parameter σ^2 as a function of temperature. Key: (□) PdOEP; (●) NiOEP; (○) CoOEP; (▲) CuOEP. The continuous lines represent fittings of eq 4 to the low-temperature data points.

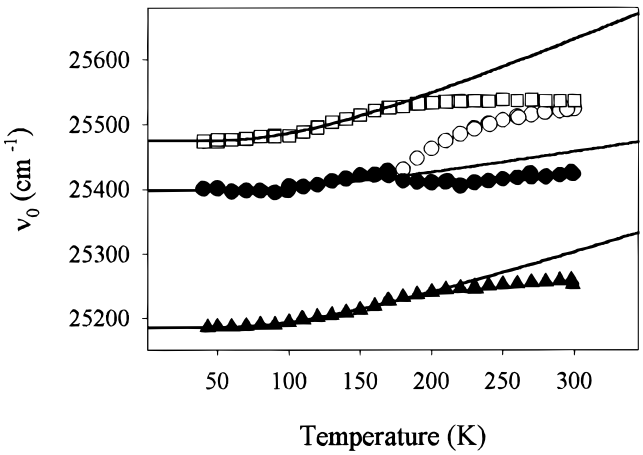

Figure 5. Values of parameter ν_0 as a function of temperature. Symbols as in Figure 4. The continuous lines represent fittings of eq 5 to the low-temperature data points.

TABLE 3: Parameters that Characterize the Low-Temperature Harmonic Behavior of the Various Metal-Octaethylporphyrins Investigated

derivative	NS	$\langle\nu\rangle$ (cm^{-1})	σ_{in} (cm^{-1})
Ni−OEP	0.08 ± 0.03	230 ± 15	0
Cu−OEP	0.08 ± 0.03	230 ± 15	0
Co−OEP	0.08 ± 0.03	230 ± 15	0
Pd−OEP	0.09 ± 0.05	230 ± 15	290 ± 20

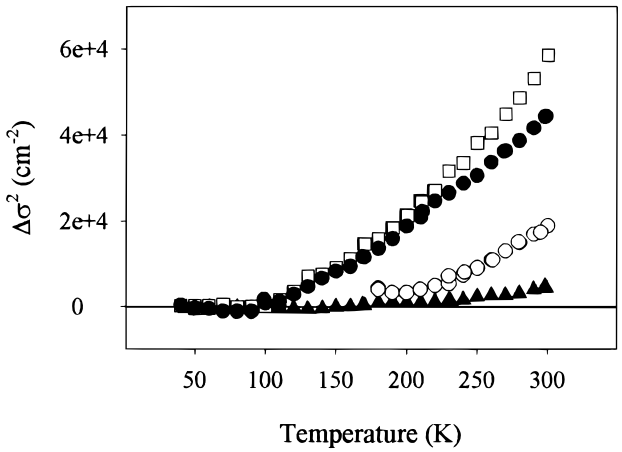

Figure 6. Deviations of parameter σ^2 from the harmonic behavior. The parameter $\Delta\sigma^2(T)$ is defined as: $\Delta\sigma^2(T) = \sigma^2(T) - \sigma^2_{harm}(T)$; see text for details. Symbols as in Figure 4.

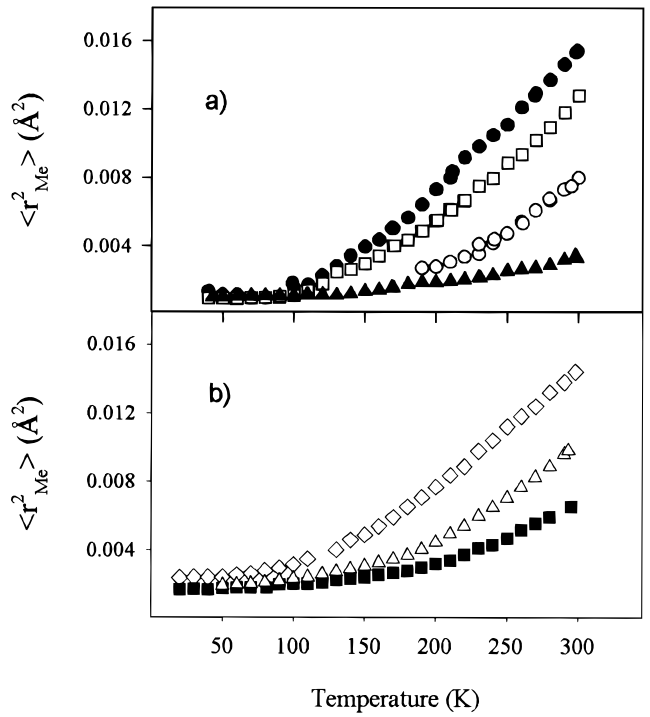

Figure 7. Mean square fluctuations of the central metal relative to the porphyrin skeleton derived from the temperature-dependent line broadening of the Soret band. (a) Metal OEPs; symbols as in Figure 4. (b) Key: (◊) Mb; (△) protoheme-CO; (■) MbCO.

motions, in relation with the glass transition of the solvent. The data depicted in Figures 4 and 6 clearly show that the magnitude of $\sigma^2(T)$ and $\Delta\sigma^2(T)$ depends dramatically on the choice of the central metal. This dependence can be expressed in quantitative terms by the $\Delta\sigma^2$ values obtained at 300 K, namely 5.9×10^4 cm^{-2} for PdOEP, 4.5×10^4 cm^{-2} for NiOEP, 1.8×10^4 cm^{-2} for CoOEP, and only 0.5×10^4 cm^{-2} for CuOEP.

It should also be noted that in addition to its large anharmonicity, PdOEP is characterized by a large inhomogeneous broadening $\sigma_{in} = 270$ cm^{-1}, implying that even at low temperatures this sample is significantly inhomogeneous.

Assignment of Low-Frequency Vibrations. The results just presented, as well as the absence of any deviations of $\sigma^2(T)$ from the predictions of the harmonic model for metal-free porphyrins,[7b] clearly show that the central metal is pivotal for the physical assessment of the employed Einstein oscillator. In the following we discuss some possible interpretations and assignments.

In a recent paper, Melchers et al.[19] combined a detailed normal coordinate analysis of CO-ligated and unligated myoglobin derivatives with studies of their optical Soret bands and of their Mössbauer spectra. The main result emerging from this study is that heme group and protein should be considered as a dynamic entity in that, in particular, iron motions contribute to the eigenvectors of several protein modes. Concerning optical absorption, the authors compared experiment and theory by calculating the mean square fluctuations (MSF) of Fe(II) with respect to the heme group first from their normal coordinates and second from the Gaussian part of the optical absorption, by identifying the Einstein oscillator with the iron motion relative to the carbons of the heme skeleton. For both Mb and MbCO, corresponding MSF values derived by normal mode calculations and optical absorption are in fairly good agreement in the low temperature harmonic regime. Above the protein/solvent glass transition (130 K for Mb, 180 K for MbCO) the MSF values derived from the optical absorption data become much larger than predicted by the normal coordinate analysis, thus indicating the onset of anharmonic structural fluctuations vibrationally coupled to the heme. This effect is significantly more pronounced for Mb than for MbCO in that the MSF value at room temperature is 0.015 Å^2 for the former and 0.006 Å^2 for the latter. The large MSF values for Mb most likely also reflect fluctuations between different conformational substates of the Fe−HisF8 linkage, which were recently inferred from an analysis of the Raman band arising from the Fe^{2+}- N_ϵ(HisF8) stretching vibration[20] and of the near-infrared absorption band III.[21] Additionally, the study of Melchers et al.[19] shows, in agreement with previous suggestions,[22] that the Fe motions probed by Mössbauer spectroscopy involve essentially the entire heme group and do not represent the relative intra-heme Fe^{2+} position.

For the porphyrins investigated in this study we have followed the approach of Melchers et al.[19] in that we identified the Einstein oscillator in eq 4 with the motions of the central metal relative to the carbons of the porphyrin skeleton.[23] Therefore, the MSF of the central metal atom ($\langle r^2_{Me}\rangle_{OPT}$) have been calculated from the Gaussian width of the Soret absorption band according to

$$\langle r_{Me}{}^2\rangle_{OPT} = \frac{h}{2m_{Me}\langle\nu\rangle}(2\pi)^2\left[\frac{\sigma^2(T) - \sigma^2_{in}}{NS\langle\nu\rangle^2}\right] \qquad (10)$$

where m_{Me} is the mass of the central metal atom and $\langle\nu\rangle$ denotes the frequency of the Einstein oscillator. Figure 7 displays the temperature-dependent MSF values of the investigated porphyrins and, for comparison, also the analogous values calculated for Mb, MbCO,[24] and protoheme-CO.[7b] The MSF values closely follow the $\sigma^2(T)$ behavior reported in Figure 5, in that anharmonic motions are large for Ni- and PdOEP, small for CoOEP, and almost absent for CuOEP. In particular, we note that central metal MSF values at room temperature relative to NiOEP and PdOEP are almost equal to those relative to Mb.

The similarity of MSF for porphyrins in an organic solvent and for Mb in aqueous solution is suggestive of an almost liquid-like behavior of the heme environment in deoxymyoglobin. The already reported[7b,24] stabilizing effect of bound CO, which significantly reduces the iron MSF, is also evident in Figure 7.

Despite the success of the approach just described in quantitatively exploring the differences between iron motions detected by optical and Mössbauer spectroscopies, it does not explain the origin of the vibronic coupling between the proposed Einstein oscillator and the electronic transition into the *B* states. This situation is in particular problematic for MbCO, for which crystallographic data have revealed an in-plane configuration of the central metal combined with a nearly perpendicular orientation of the proximal imidazole. In fact, the iron motion has an in-plane and an out-of-plane component; if one assumes D_{4h} symmetry,[25] the former must be part of a low-frequency E_u mode of the macrocycle, whereas the latter contributes to doming motions of A_{2u} symmetry. For both, vibronic transitions into the *B* states that involve the creation or annihilation of an odd number of vibrational quanta (i.e., with $n_j = 1, 3, 5, .., 2k+1$) are symmetry forbidden, whereas those with $n_j = 2, 4, 6, .., 2k$ are allowed. The situation is different for Mb, in which the heme is nonplanar, due to doming and waving distortions,[26] with a significant Fe^{2+} displacement from the mean heme plane. These distortions may give rise to Franck−Condon activity of A_{2u} and E_u modes even for an odd number of vibrational quanta. One therefore expects that the effective frequency of the Einstein oscillator derived from the fit to the Soret band should be larger for MbCO than for Mb. Indeed, Cupane et al.[24] obtained $\langle\nu\rangle = 140\ cm^{-1}$ for the latter and $\langle\nu\rangle = 180\ cm^{-1}$ for the former. Moreover, protein/solvent harmonic motions of the appropriate symmetry could also contribute to the aformentioned Einstein oscillator.

The model porphyrins investigated in the present study are either planar (CuOEP, CoOEP) or slightly ruffled (one conformer of NiOEP). In all cases, only Franck−Condon transitions with even n_j are allowed for A_{2u} and E_u motions of the metal. This notion is consistent with the comparatively high effective frequency value of 230 cm^{-1} obtained for the Einstein oscillator of all the porphyrins investigated.

We are now left with the question of how to explain the different degree of anharmonicity displayed by the different metals. As mentioned in our earlier paper,[7a] the deviation from harmonic behavior observed for NiOEP is of the same order of magnitude as that obtained for heme proteins. This results suggests that coupling to the solvent is very effective even though it is solely governed by nonbonding interactions with molecules in the solvation shell, whereas in hemeproteins the central metal atom is covalently linked to the protein environment. On the other hand, the solvent is known to provide a rich phonon spectrum in the low-frequency region.[27] These motions become certainly anharmonic in the liquid phase (above the glass transition temperature) and the nonbonding interactions just mentioned are apparently capable of imposing this anharmonicity onto the motion of the porphyrin metal. The efficiency of this process, however, depends on the strength of the ligand field of the four pyrrole nitrogens. Cu(II) and Co(II) are known to fit well into the central hole of the porphyrin (ionic radii in square planar coordination are reported to be 0.68 and 0.71 Å, respectively[29]), and are therefore tightly bound. Consequently, both distortions from D_{4h} symmetry and metal out-of-plane motions need more energy and therefore a small anharmonicity is observed only at high temperatures. The situation is different for Pd(II) and Ni(II). In the case of PdOEP, out-of-plane positions of the metal and consequently doming of the porphyrin occur more easily, due to the larger ionic radius of the metal (0.78 Å[29]); as a consequence, a much larger anharmonicity is observed. An inhomogeneous distribution of metal out-of-plane equilibrium positions, on the other hand, could well explain the large inhomogeneous broadening of the Soret band observed even at low temperatures. On the contrary, in the case of NiOEP, distortions from D_{4h} symmetry may occur because of the smallness of the central metal (ionic radius 0.61 Å[29]); indeed, nonplanar distortions (ruffling or saddling[28]) are promoted by small metals because the distortion allows the porphyrin core to contract around the metal, giving metal−nitrogen bond lengths closer to the "optimum" values. Consistently, both the conformation-sensitive ν_{10} Raman line and the optical absorption Soret band appear to be composed of different subbands (resulting from planar and ruffled conformers) only in the case of NiOEP, wheras they remain homogeneous for the other porphyrins. The narrow and homogeneous ν_{10} line observed in the resonance Raman spectrum of PdOEP (see Figure 1) implies that for this porphyrin, the out-of-plane distortion responsible for the large anharmonicity and spectral inhomogeneity is predominantly doming, which is not expected to affect the core size marker frequencies.[28]

Conclusions

We have investigated the vibrational coupling of the Soret band of several metal-OEPs in organic solvents by optical absorption and resonance Raman spectroscopies with the aim of studying the conformational flexibility of these biologically relevant molecules. Following an approach already proposed in the literature,[19] the MSF of the central metal atom with respect to the porphyrin plane have also been obtained from the temperature dependence of the Gaussian width of the Soret band. From our study, metal-OEPs appear to be characterized by the following kinds of motions:

(1) High- and low-frequency harmonic vibrations. The former are essentially the well-known A_{1g} porphyrin modes giving rise to the prominent bands in the resonance Raman spectra. The latter are A_{2u} and E_u motions of the metal and of the porphyrin, as well as harmonic vibrations of the solvent molecules contributing to the "bath" of low-frequency modes.

(2) Anharmonic motions become apparent at temperatures above the solvent matrix glass transition and contribute essentially to the central metal-porphyrin MSF observed at room temperature. These motions are mainly solvent motions that become anharmonic in the liquid phase and are transmitted to the motion of the metal-porphyrin system through nonbonded interactions. The efficiency of this coupling, however, depends dramatically on the size and electronic structure of the central metal and specifically on the strength of the ligand field experienced by the metal. The difference between Ni(II)-OEP and Cu(II)-OEP is particularly striking because anharmonic contributions to MSF are large for the former and almost negligible for the latter. Moreover, MSF observed for Ni(II)-OEP are of the same magnitude as those previously reported for deoxy myoglobin.

We may speculate on the biological relevance of the findings just summarized. Indeed, a large conformational flexibility may be necessary in iron-containing hemeproteins to optimize the fine-tuning of binding and release of exogenous ligands. On the contrary, the reduced flexibility found for Cu-OEP seems to be characteristic also of other copper-containing metalloproteins active stes like, for example, superoxide dismutase.[30] Hence, one may suppose that reduced flexibility is required for

active sites, which are usually involved in electron-transfer reactions, to increase their efficiency.

Acknowledgment. A. C. and M. L. thank Mr. G. Lapis and Mr. F. D'Anca for technical support. This work was financially supported by the European Community in the framework of the network program: "The dynamics of protein structure", which was part of the "Human Capital and Mobility Program". Further support was provided by grants from the Italian "Ministero della Pubblica Istruzione" (MPI 60%) and from the "Forschungsnachwuchskommission" of the Universität Bremen.

References and Notes

(1) *The Porphyrins*; Dolphin, D., Ed.; Academic: New York, 1978; Vols. I−VI.

(2) Fox, M. A.; Oan, H.-L; Jones, W. E., Jr., Melamed, D. *J. Phys. Chem.* **1995**, *99*, 11523.

(3) (a) Shelnutt, J. A., Medforth, C. J., Berber, M. D., Barkigia, K. M.; Smith, K. M. *J. Am. Chem. Soc.* **1991**, *113*, 4077. (b) Jentzen, W., Simpson, M. C.; Hobbs, J. D; Song, X.-Z.; Ema, T.; Nelson, N. Y.; Medforth, C. J.; Smith, K. M.; Veyrat, M.; Mazzanti, M.; Ramasseul, R.; Marchon, J. C.; Takeuchi, T.; Goddard, W., III; Shelnutt, J. A. *J. Am. Chem. Soc.* **1995**, *117*, 11085.

(4) Jentzen, W.; Song, X.-Z.; Shelnutt, J. A. *J. Phys. Chem. B.* **1997**, *101*, 1684.

(5) (a) Di Pace, A.; Cupane, A.; Leone, M., Vitrano, E.; Cordone, L. *Biophys. J.* **1992**, *63*, 475. (b) Cupane, A.; Leone, M.; Vitrano, E. *Eur. Biophys. J.* **1993**, *21*, 385. (c) Cupane, A.; Leone, M.; Vitrano, E.; Cordone, L.; Hiltpold, U. R.; Winterhalter, K. H.; Yu, W.; Di Iorio, E. E. *Biophys. J.* **1993**, *65*, 2461.

(6) (a) Harris, C. B., Shelby, R. M.; Cornelius, P. A. *Phys. Rev. Lett.* **1977**, *38*, 1415. (b) Schweitzer-Stenner, R.; Jentzen, W.; Dreybrodt, W. In *"Fifth International Conference on the Spectroscopy of Biological Molecules;* Theophanides, T.; Anastassopoulou, J.; Fotopoulos, N., Eds.; Kluver Academic: Dordrecht, The Netherlands, 1993; p 31.

(7) (a) Cupane, A.; Leone, M.; Cordone, L.; Gilch, H.; Dreybrodt, W.; Unger, E.; Schweitzer-Stenner, R. *J. Phys. Chem.* **1996**, *100*, 14192. (b) Leone, M., Cupane, A.; Militello, V.; Cordone, L. *Eur. Biophys. J.* **1994**, *23*, 349.

(8) Jentzen, W.; Unger, E.; Karvounis, G.; Shelnutt, J. A.; Dreybrodt, W.; Schweitzer-Stenner, R. *J. Phys. Chem.* **1996**, *100*, 14184.

(9) Unger, E.; Dreybrodt, W.; Schweitzer-Stenner, R. *J. Phys. Chem. A.* **1997**, *101*, 5997.

(10) Schweitzer-Stenner, R.; Stichternath, A.; Dreybrodt, W.; Jentzen, W.; Song, X.-Z.; Shelnutt, J. A.; Faurskov-Nielsen, O.; Medforth, C. J.; Smith, K. M. *J. Chem. Phys.* **1997**, *107*, 1794.

(11) Cordone, L.; Cupane, A.; Leone, M.; Vitrano, E. *Biophys. Chem.* **1986**, *24*, 259.

(12) Unger, E.; Bobinger, U.; Dreybrodt, W.; Schweitzer-Stenner, R. *J. Phys. Chem.* **1993**, *97*, 9956.

(13) (a) Stallard, B. R.; Champion, P. M.; Callis, P. R.; Albrecht, A. C. *J. Chem. Phys.* **1983**, *78*, 712. (b) Rush, T. III, Kumble, R.; Mukerjee, A.; Blackwood, M. E., Jr.; Spiro, T. G. *J. Phys. Chem.* **1996**, *100*, 12076.

(14) Hizhnyakov, V.; Tehver, I. *Phys. Stat. Sol.* **1967**, *21*, 755.

(15) Hizhnyakov, V.; Tehver, I. *J. Raman Spectrosc.* **1988**, *19*, 383.

(16) Unger, E. Doctoral Thesis, University of Bremen, 1996.

(17) (a) Kim, D. H.; Kirmaier, C.; Holten, D. *Chem. Phys.* **1983**, *75*, 305. (b) Kruglik, S. G.; Apanasevich, P. A.; Chirvony, V. S.; Kvach, V. V.; Orloich, V. A. *J. Phys. Chem.* **1995**, *99*, 2978. (c) Drain, C. M.; Kirmaier, C.; Medforth, C. J.; Nurco, D. J.; Smith, K. M.; Holten, D. *J. Phys. Chem.* **1996**, *100*, 11984.

(18) (a) Bangcharoenpaurpong, O.; Schomacker, K. T.; Champion, P. M. *J. Am. Chem. Soc.* **1984**, *106*, 5688. (b) Schomacker, K. T.; Champion, P. M. *J. Chem. Phys.* **1986**, *84*, 5314.

(19) Melchers, B.; Knapp, E. W.; Parak, F.; Cordone, L.; Cupane, A.; Leone, M. *Biophys. J.* **1996**, *70*, 2092.

(20) Gilch, H.; Dreybrodt, W.; Schweitzer-Stenner, R. *Biophys. J.* **1995**, *69*, 214.

(21) Gilch, H.; Schweitzer-Stenner, R.; Dreybrodt, W.; Leone, M.; Cupane, A.; Cordone, L. *Int. J. Quantum Chem.* **1996**, *59*, 301.

(22) Parak, F.; Knapp, E. W.; Kucheida, D. *J. Mol. Biol.* **1982**, *161*, 177.

(23) In principle, this provides an upper limit for the MSF of the central metal atom because the metal displacement is part of a doming motion of the macrocycle [i.e., the A_{2u}-type vibration (γ_8)], which also involves out-of-plane displacements of the pyrrole atoms (see Li, X.-Y.; Czernuszewics, R. S.; Kincaid, J. R.; Spiro, T. G. *J. Phys. Chem.* **1990**, *94*, 31).

(24) Cupane, A.; Leone, M.; Vitrano, E.; Cordone, L. *Eur. Biophys. J.* **1995**, *23*, 385.

(25) Very recent reinvestigations of the crystal structure of Mb and MbCO (ref 26) revealed that even the heme group in MbCO is not totally planar. This finding does not seriously affect our considerations, however, because these distortions are significantly smaller than those observed for Mb and do not cause a significant metal displacement with respect to the pyrrole nitrogens.

(26) Jentzen, W.; Ma, J. G.; Shelnutt, J. A. *Biophys. J.* **1998**, *74*, 753.

(27) Harris, R. A.; Mathies, R. A.; Pollard, W. T. *J. Chem. Phys.* **1986**, *85*, 3744.

(28) Anderson, K. K.; Hobbs, J. D.; Luo, L.; Stanley, K. D.; Quirke, J. M. E.; Shelnutt, J. A. *J. Am. Chem. Soc.* **1993**, *115*, 12346.

(29) Huhney, J. E. *Inorganic Chemistry. Principles of Structure and Reactivity;* Harper and Row: New York, 1978.

(30) (a) Cupane, A.; Leone, M.; Militello, V.; Stroppolo, M. E.; Polticelli, F.; Desideri, A. *Biochemistry* **1994**, *33*, 15103. (b) Cupane, A.; Leone, M.; Militello, V.; Stroppolo, M. E.; Polticelli, F.; Desideri, A. *Biochemistry* **1995**, *34*, 16313.